CHAPTER IV

Results and Discussion

In this chapter, the results are divided into three sections. The first section mainly focuses on the synthesis and characterization of random and block copolymers of poly(*N*-isopropylacrylmide) (PNIPAAm) having multiple reactive units along their backbone such as *N*-acryloxysuccinimide (NAS) and pentafluorophenylacrylate (PFPA) by RAFT polymerization. The second section explains the ability of random and blocks copolymers to form fibers and micelles, respectively. The last section is dedicated to the evaluation of cellular response of the fiber mats.

4.1 Preparation of P(NIPAAm-*r*-NAS) by RAFT polymerization

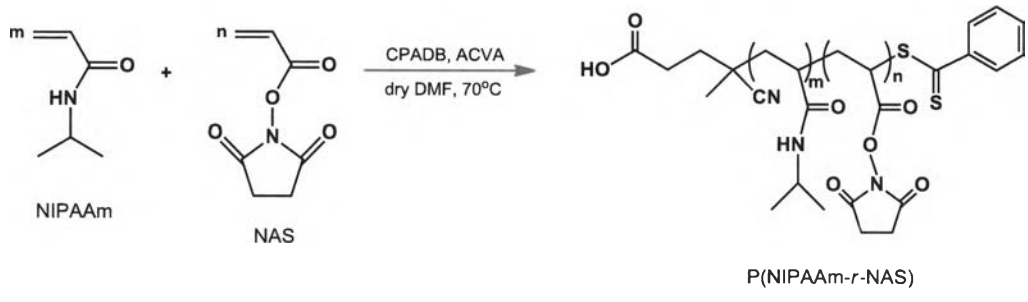

Figure 4.1. Synthetic pathway of P(NIPAAm-*r*-NAS) by RAFT polymerization.

The synthesis of P(NIPAAm-*r*-NAS) was performed by RAFT polymerization in anh. DMF at 70°C using CPADB as a chain transfer agent (CTA) and ACVA as a radical initiator (Figure 4.1). Table 4.1 gives an overview of the reaction conditions and the molecular weight information of copolymers prepared by RAFT polymerizations under different conditions. A ratio of [CTA]/[I] was fixed at 4/1, while the ratios of [M]/[CTA] and comonomer ratios were varied. As demonstrated in Table 4.1, the copolymer composition ratio between NIPAAm and NAS can be precisely controlled as a function of the comonomer in the feed. The molecular weight of the copolymers could be raised by an increment of the [M]/[CTA] ratio. Moreover, the

ratio of [CTA]/[I] played an important role in controlling molecular weight and PDI as shown in Table 4.2. PDI decreased with an increasing [CTA]/[I] ratio from 3/1 to 4/1. In all cases, the molecular weights were ranging from 16.8 to 44.8 and the PDI of the copolymers was between 1.11 and 1.28.

Table 4.1 Summary of reaction conditions and molecular weight information of P(NIPAAm-*r*-NAS) copolymers synthesized by RAFT polymerization.

[M]/[CTA]	Molar ratio [NIPAAm]:[NAS]	[CTA]/[I]	M_n (kDa)	M_w (kDa)	PDI	Copolymer composition of PNIPAAm:PNAS
400	90:10	4	43.9	55.6	1.27	91:9
	80:20		47.8	66.0	1.38	82:18
	70:30		ND	ND	ND	73:27
	60:40		ND	ND	ND	64:36
600	90:10		74.6	97.0	1.30	91:9

*ND = Not Detectable by GPC measurement

Table 4.2 Characteristics of the synthesized copolymers (target DP = 400, comonomer feed ratio of [NIPAAm]:[NAS] = 90:10) as a function of [CTA]/[I] ratio.

Time (h)	[CTA]/[I] = 3			[CTA]/[I] = 4		
	M_n (kDa)	M_w (kDa)	PDI	M_n (kDa)	M_w (kDa)	PDI
2	19.3	22.4	1.16	16.8	19.2	1.14
4	32.8	39.5	1.20	37.7	42.0	1.11
6	37.3	46.1	1.24	42.6	47.8	1.12
8	42.6	52.8	1.24	44.8	51.9	1.16
10	42.5	54.2	1.28	44.1	51.9	1.18

The kinetic plots for the RAFT polymerization of P(NIPAAm-*r*-NAS) (Figure 4.2) shows that molecular weight increases linearly with polymerization time within the first 6 h implying that a constant number of propagating radicals or chain transfer equilibrium condition was maintained throughout the duration of polymerization for 6 h.

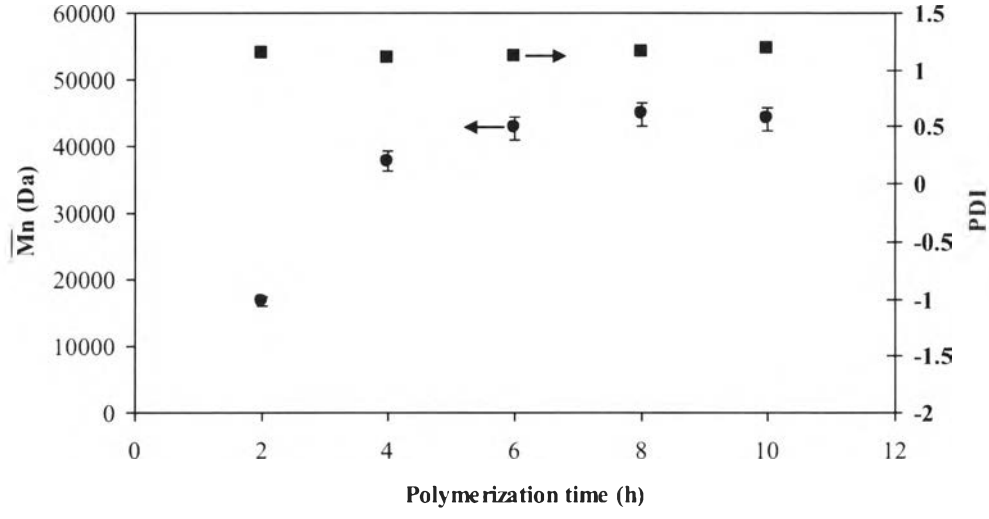

Figure 4.2. Plots of molecular weight (M_n) and PDI versus polymerization time for molar ratio of [M]/[CTA] = 400, and [CTA]/[I] = 4 in the polymerization of P(NIPAAm-*r*-NAS) (90/10) in anh. DMF at 70°C.

The success of P(NIPAAm-*r*-NAS) formation was also confirmed by ^{1}H NMR and FT-IR analyses as shown in Figure 4.3 and 4.4, respectively. The characteristic signals of both PNIPAAm (the proton on isopropyl group [-C<u>H</u>-$(CH_3)_2$] at δ ~3.6-4.0 ppm) and PNAS segments (four protons of succinimide group at δ ~2.6-3.0 ppm) appear in the spectrum of the copolymer as shown in Figure 4.3. The characteristic bands of both NAS unit (succinimide groups at 1810, 1781, and, 1733 cm^{-1}) and NIPAAm unit (C=O stretching (Amide I) at 1658, N-H stretching (Amide II) at 1549 cm^{-1}) appeared clearly in the FT-IR spectrum of the P(NIPAAm-*r*-NAS) copolymer (Figure 4.4).

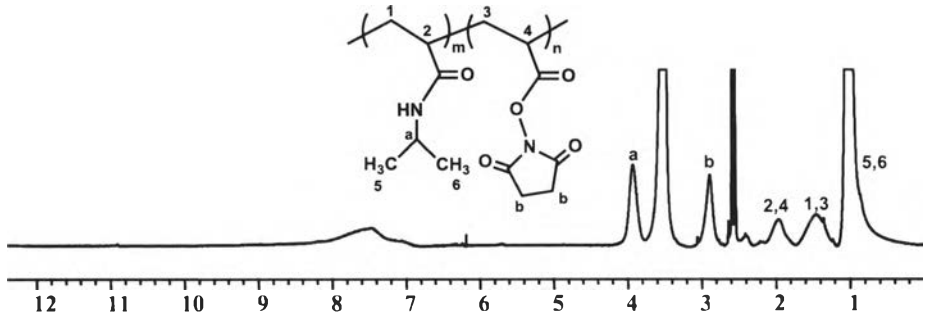

Figure 4.3. ^{1}H NMR spectrum of P(NIPAAm-*r*-NAS) copolymer.

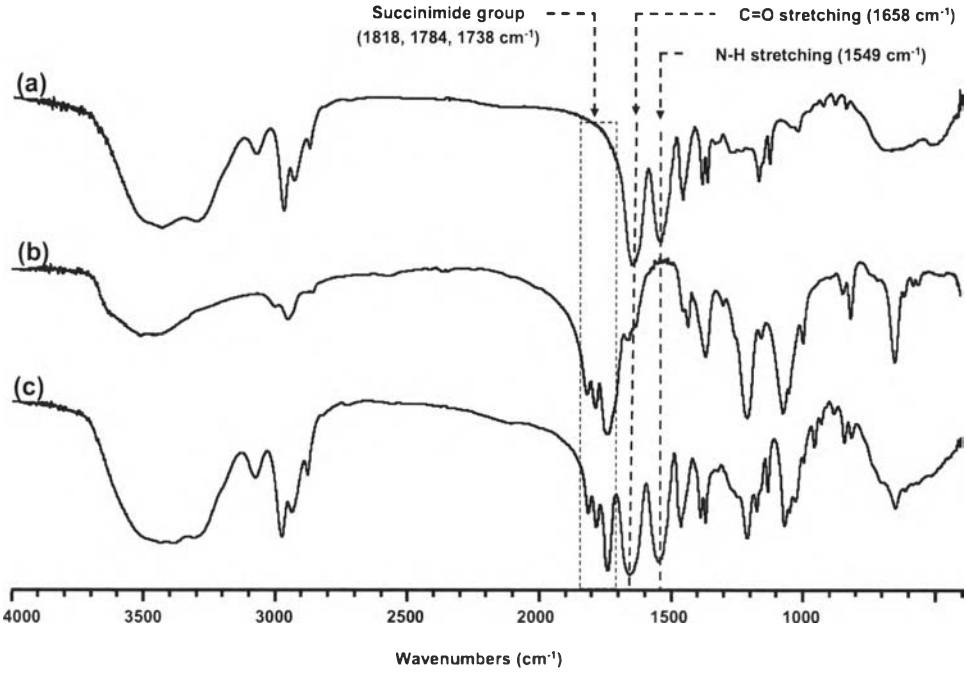

Figure 4.4. FT-IR spectra of (a) PNIPAAm, (b) PNAS, and (c) P(NIPAAm-*r*-NAS) copolymer.

4.2 Preparation of PPFPA by RAFT polymerization

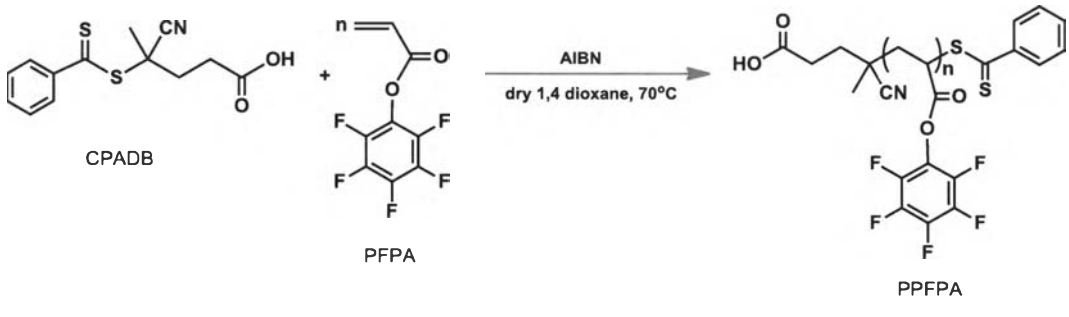

Figure 4.5. Synthetic pathway of PPFPA by RAFT polymerization.

PPFPA homopolymer was synthesized by RAFT polymerization utilizing CPADB as a CTA and AIBN as an initiator in dry 1,4-dioxane at 70°C (Figure 4.5). In this study, ratios of [M]/[CTA] and [CTA]/[I] were fixed at 500/1 and 10/1, respectively. Figure 4.6 shows the relationships between molecular weight and monomer conversion of PPFPA in this experiment. The molecular weight of polymer linearly increased with

monomer conversion. These results fully confirm that the polymerization process proceeded via a controlled mechanism. Moreover, the success of PPFPA synthesis could also be verified by the appearance of C=O stretching band at 1783 cm^{-1} corresponding to the reactive ester, C=C bending band at 1515 cm^{-1} corresponding to aromatic ring, and C-O ester band at 1090 cm^{-1} as shown in Figure 4.7.

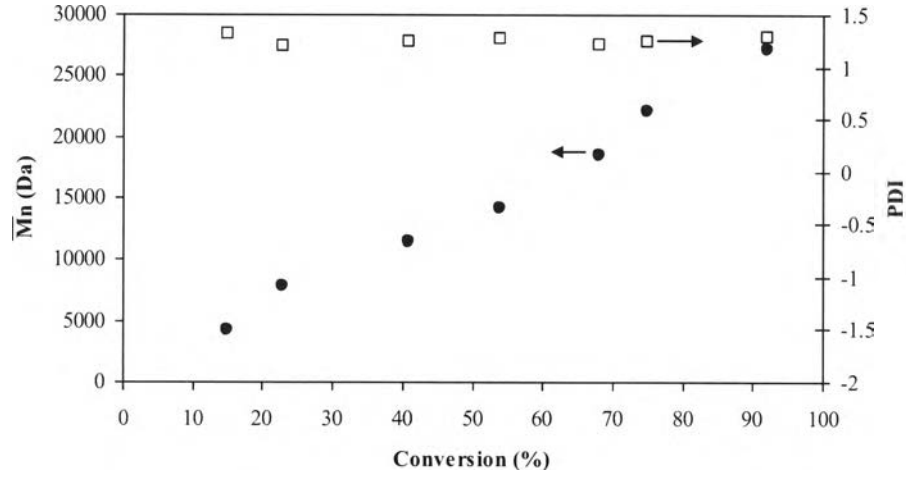

Figure 4.6. Plots of molecular weight (M_n) and PDI as a function of monomer conversion for the RAFT polymerization of PFPA.

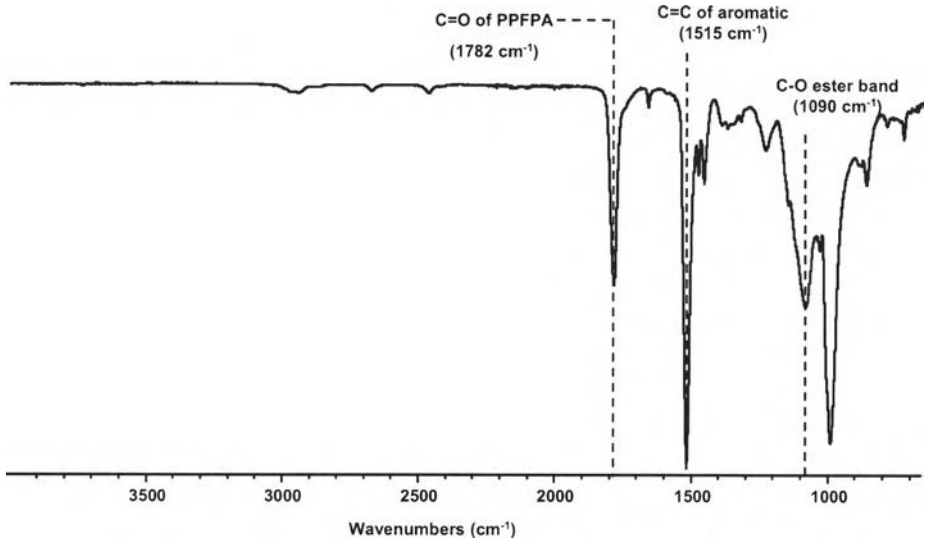

Figure 4.7. FT IR spectrum of PPFPA.

4.3 Preparation of PPFPA-*b*-PNIPAAm by RAFT polymerization

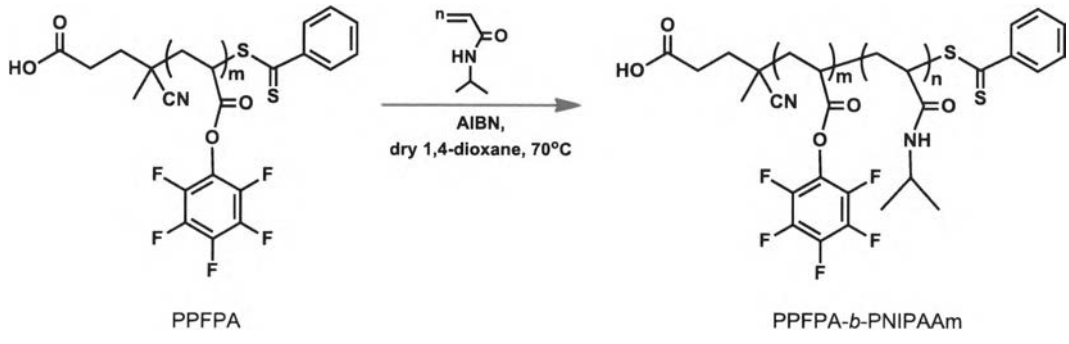

Figure 4.8. Synthetic pathway of PPFPA-*b*-PNIPAAm by RAFT polymerization.

For the synthesis of diblock copolymers of PPFPA-*b*-PNIPAAm using RAFT polymerization, it is advisable to start with the monomer that shows higher transfer ability for the selected CTA. In this case, PFPA was first synthesized and used as a macro CTA for PNIPAAm synthesis [29] (Figure 4.8). The PPFPA macro-CTAs with two molecular weights of 6.5 and 22.1 kDa were prepared (see Table 4.3). GPC chromatograms of the PPFPA and diblock copolymers are shown in Figure 4.9. A single peak was observed for each of the polymers, and a decrease in retention time as well as progressive peak broadening is seen with each block addition. The PPFPA with the two molecular weights of 6.5 and 22.1 kDa showed a good control of PDI and yielded block copolymer of the PPFPA-*b*-PNIPAAm with molecular weights of 11.5 kDa and 30.4, respectively. However, the GPC chromatogram of the resulting block copolymer having the molecular weight of 30.4 kDa has a slight shoulder as a result of terminated chains. Additionally, Table 4.3 gives an overview of the molecular weight information of the block copolymers prepared by RAFT polymerizations. The molecular weight (M_n) of the block increased with increasing [monomer]/[PPFPA macro-CTA] ratio. The content of the NIPAAm in the block copolymer was determined from ^{1}H NMR data by selecting the areas of the signals at 4.10 ppm (for methine proton of NIPAAm) in relation to the area of the signal at 3.10 ppm of the PPFPA polymer backbone. The contents of NIPAAm in the block copolymers were 74 and 77 mol% for the PPFPA-CTA with M_n of 6.5 and 22.1 kDa, respectively.

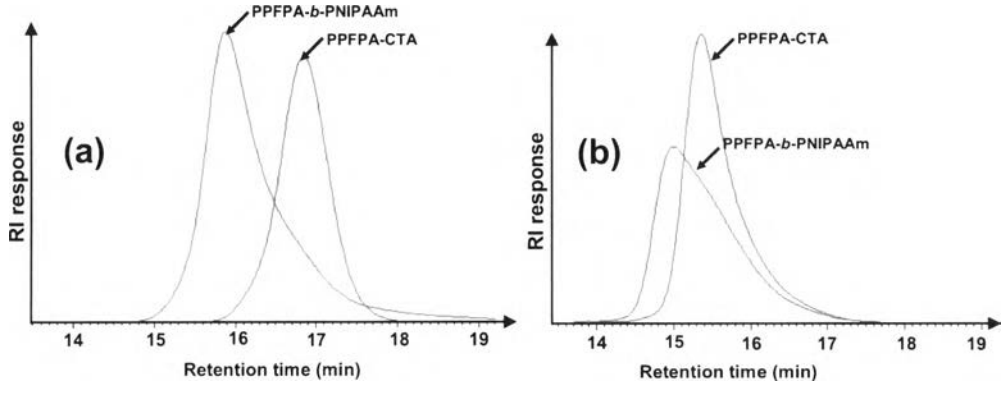

PPFPA, M_n = 6.5 kDa, PDI = 1.10
PPFPA-*b*-PNIPAAm, M_n = 11.5 kDa, PDI = 1.30

PPFPA, M_n = 22.1 kDa, PDI = 1.30
PPFPA-*b*-PNIPAAm, M_n = 30.4 kDa, PDI = 1.36

Figure 4.9. GPC traces of PPFPA molecular weights of 6.5 kDa (a) and 22.1 kDa (b) and their corresponding block copolymers.

Table 4.3 Molecular weight information of PPFPA-*b*-PNIPAAm copolymers synthesized by RAFT polymerization.

First block				PPFPA-*b*-PNIPAAm				
Macro-CTA	M_n (kDa)	M_w (kDa)	PDI	M_n (kDa)	M_w (kDa)	PDI	NIPAAm (mol-%)	PPFPA (mol-%)
PPFPA-CTA	6.5	7.1	1.10	11.5	14.9	1.30	74	26
	22.1	28.7	1.30	30.4	41.3	1.36	77	23

^{1}H NMR measurement proved a successful formation of the block copolymers as shown in Figure 4.10. The characteristic proton signals of PPFPA at 3.10, 2.50, and 2.12 ppm attributed to CH and CH_2 groups of polymer backbone. The chain extension of the second block of PNIPAAm was confirmed by the appearance of a new signal at 4.10 ppm attributed to $-C\underline{H}(CH_3)_2$ of the methine proton of NIPAAm. The combination of a single GPC peak and the presence of characteristic protons for both PPFPA and PNIPAAm lead to the conclusion that diblock PPFPA-*b*-PNIPAAm copolymers were successfully synthesized.

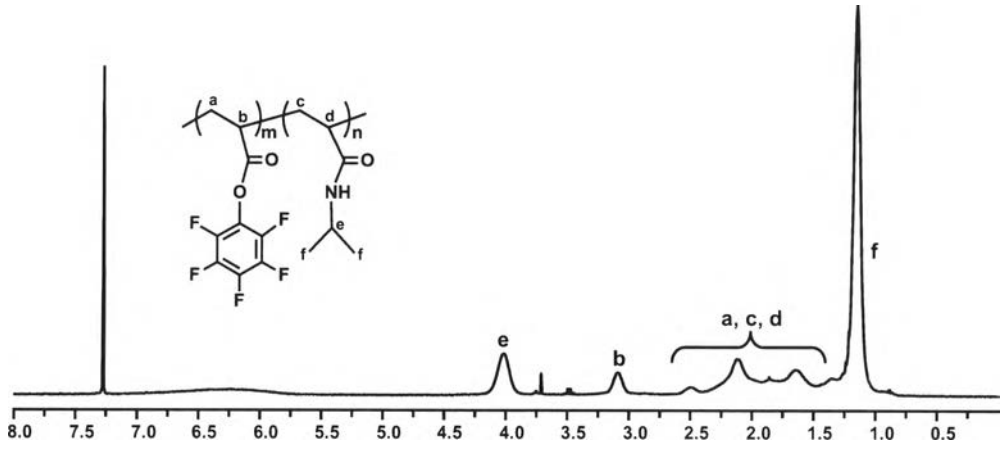

Figure 4.10. ^{1}H NMR spectrum of PPFPA-*b*-PNIPAAm in $CDCl_3$.

4.4 Post polymerization modification of activated ester copolymers with ONB-protected diamine

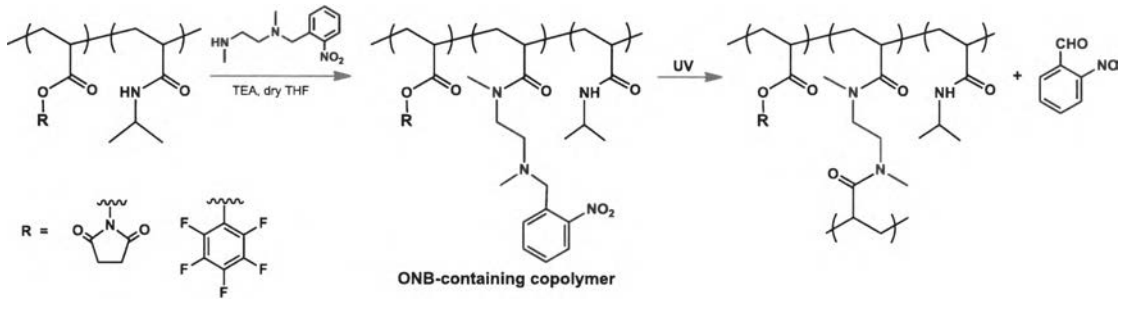

Figure 4.11. Schematic representation of the nucleophilic substitution of activated ester copolymers with ONB-protected diamine.

Herein, light responsive moieties of ONB containing random and block copolymers were prepared via post polymerization modification of activated ester parts (NAS and PFPA unit) with a mono ONB-protected diamine. Upon UV irradiation at 365 nm, the ONB protected amine group should be released, which can subsequently induce cross-linking via activated ester-amine chemistry resulting in a network formation as shown in Figure 4.11. A successful reaction can be demonstrated by the results from ^{1}H NMR and FTIR analysis.

The ONB containing P(NIPAAm-*r*-NAS) copolymer was synthesized via post polymerization modification of ONB-protected diamine with NAS moieties. In this study, the precursor copolymer, P(NIPAAm-*r*-NAS) was first synthesized by RAFT polymerization. The mole ratio of [M]/[CTA], [NIPAAm]/[NAS], and [CTA]/[I] were fixed at 1000/1, 500/500, and 4/1, respectively in order to get the copolymer with high molecular weight in order to assure electrospinnability. As calculated from ^{1}H NMR of which spectrum is displayed in Figure 4.12 (a), the theoretical molecular weight ($M_{n,th}$) of the precursor copolymer was 133.6 kDa and the copolymer composition ratio between NIPAAm and NAS (50:50) closely resembled to the comonomer in the feed (50:50). The conversion of the parent PNAS in the copolymer to the corresponding ONB-protected amine was also determined by ^{1}H NMR (Figure 4.12 (b)). The characteristic signal of the four aromatic protons of the ONB moieties in a range of δ=7.49-7.85 ppm clearly confirmed the attachment of the ONB groups to the random copolymer. The amount of the incorporated ONB-protected groups onto the copolymer was found to be 21.9%.

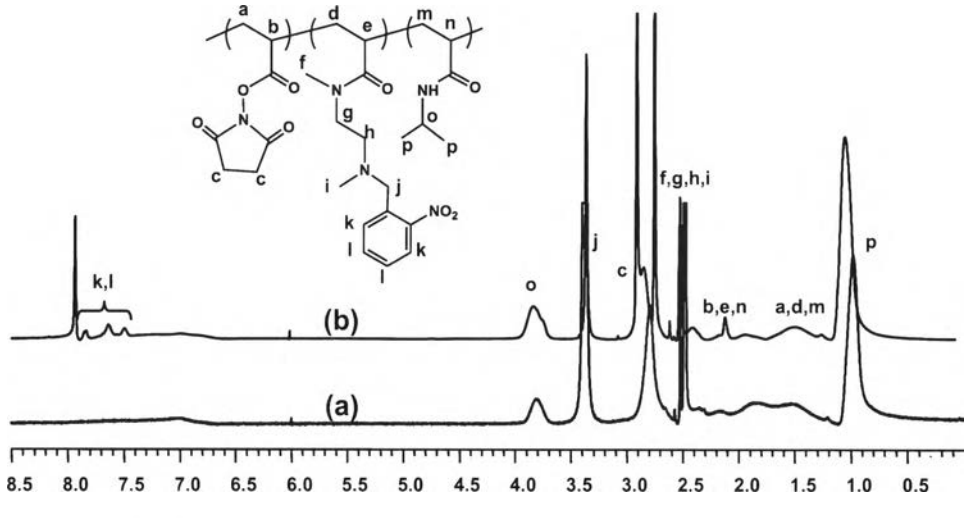

Figure 4.12. ^{1}H NMR spectra of P(NIPAAm-*r*-NAS) copolymer in DMSO-d_6 (a) before and (b) after a reaction with ONB-protected diamine.

The ONB containing PPFPA-*b*-PNIPAAm copolymer was also synthesized via post polymerization modification of PFPA moieties. Figure 4.16 (b) represents ^{1}H NMR

spectrum of ONB containing block copolymer of PPFPA-*b*-PNIPAAm. The signals of the four aromatic protons of the ONB moieties in a range of δ=7.52-8.09 ppm clearly confirmed the attachment of the ONB groups to the block copolymer. The amount of incorporated ONB-protected amine in the copolymer can be calculated by ^{1}H NMR from the relative ratio between the peak integration of the four aromatic protons and the peak integration of one proton at 3.10 ppm of the PPFPA polymer backbone. The amount of the incorporated ONB amine onto PPFPA-*b*-PNIPAAm was found to be 20.7%. Additionally, the successful conversion of the parent PPFPA in the copolymer to the corresponding ONB-protected group was also confirmed by FTIR analysis from the decrement of C=O peak at 1782 cm^{-1} of PPFPA and the increment of the amide carbonyl group at 1645 cm^{-1} (Figure 4.17 (b)). After the post polymerization modification, the molecular weight of the ONB containing block copolymer was slightly shifted to higher molecular weight in comparison to the GPC trace of the precursor block copolymer due to the increment of molecular weight per repeating unit (See Appendices Figure B-1).

4.5 Preparation of cross-linked polymeric micelles of PPFPA-*b*-PNIPAAm

In this part, we introduce a new methodology for polymeric micelles preparation from diblock copolymer having PPFPA moieties as hydrophobic parts, PNIPAAm as hydrophilic part, and ONB-protected diamine as a photo-induced cross-linker molecule of which the strategy is shown in Figure 4.13. The molecular weight of PPFPA-*b*-PNIPAAm block copolymers and the cross-linked density were fixed at around 30 kDa, and 20%, respectively, while the copolymer compositions of PPFPA: PNIPAAm were varied from 23:77 and 71:29.

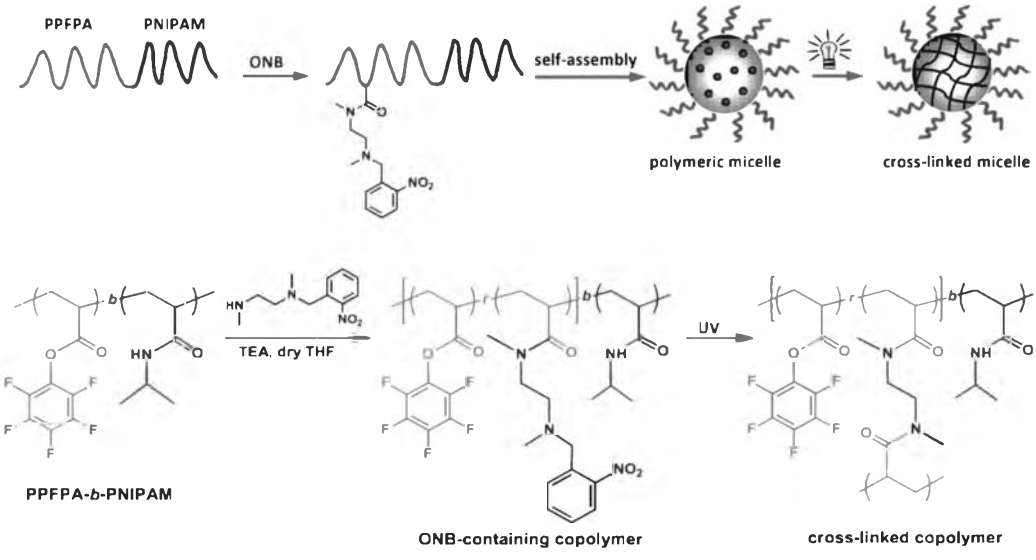

Figure 4.13. Schematic representation of the partial substitution of PPFPA-*b*-PNIPAM copolymers with ONB-protected diamine.

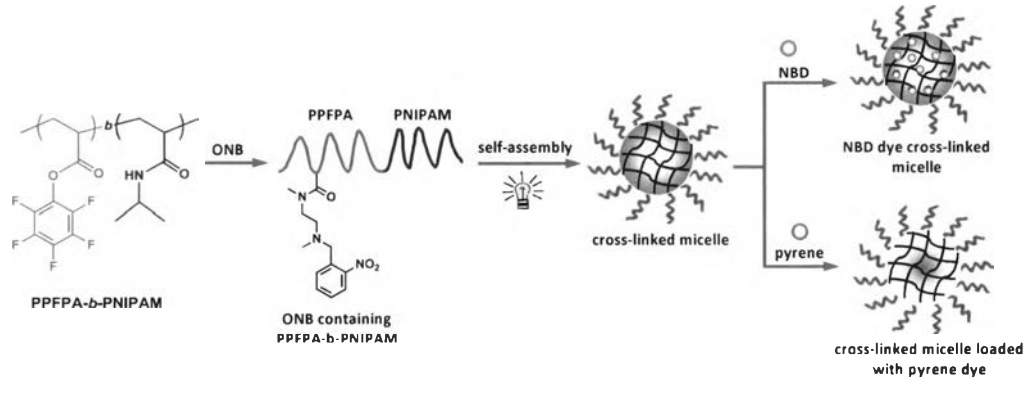

Figure 4.14. Schematic representation of design and synthesis of NBD dye cross-linked polymeric micelles and cross-linked micelle loaded with pyrene dye.

Micellization of the diblock copolymers in aqueous solution was characterized by dynamic laser scattering (DLS) and transmission electron microscopy (TEM). DLS studies (Table 4.4) revealed that the size of both uncross-linked and cross-linked micelles above the lower critical solution temperature (LCST) became smaller than that below the LCST due to the outer shell of PNIPAM dehydrated and collapsed. After UV irradiation at 365 nm, the average size of the cross-linked micelles were found to be slightly smaller than those of uncross-linked micelles

implying that covalently cross-linked network of ONB-protected amine with the PPFPA part in the core were formed. Moreover, the average size of the micelles having a copolymer composition of PPFPA: PNIPAAm of 71:29 is smaller than that with the ratio of PPFPA:PNIPAAm of 23:77 implying that the size of the micelles corresponds with the length of the PNIPPAm outer shell. In addition, size distribution profiles measured by DLS showed that all of the micelles have a unimodal size distribution. The micelles did not precipitate above the LCST because the DLS measurement was carried out at a very low concentration (1 mg/mL) allowing us to determine their size by DLS. TEM images revealed well-defined spherical shapes with slightly smaller diameters than those observed in DLS, which is attributed to the shrinkage of the micelles after solvent evaporation during TEM sample preparation (Figure 4.15). NBD dye conjugate was incorporated onto the residual PFPA moiety in the core of the cross-linked micelles to demonstrate the possibility for additional post functionalization modification (Figure 4.14). A successful incorporation of NBD dye was confirmed by ^{1}H NMR and FTIR as shown in Figure 4.16 (c) and 4.17 (c), respectively. The disappearance of activated carbonyl group at 1782 cm^{-1} and appearance of amide carbonyl group at 1646 cm^{-1} suggest that the PFPA unit was completely converted to amide when NBD dye was reacted with PFPA. Similar explanation can also be applied for the ^{1}H NMR spectrum. The signals of the two aromatic protons of the NBD in a range of δ=7.29-8.20 ppm clearly confirmed the attachment of the NBD to the block copolymer.

Table 4.4 Summary of average sizes of PFPA-*b*-PNIPAAm, cross-linked PFPA-*b*-PNIPAAm, and NBD dye cross-linked PFPA-*b*-PNIPAAm micelles.

PPFPA:PNIPAAm (% mol ratio)	Average size (nm)					
	PPFPA-*b*-PNIPAAm		Cross-linked PPFPA-*b*-PNIPAAm		NBD dye cross-linked PPFPA-*b*-PNIPAAm	
	10°C	40°C	10°C	40°C	10°C	40°C
23:77 (M_n= 30.4 kDa)	257.23±4.59	178.15±2.21	183.23±1.85	128.97±1.10	211.57±2.74	162.90±0.62
71:29 (M_n= 32.5 kDa)	122.40±3.04	81.22±0.17	75.19±2.12	64.48±0.31	82.19±1.02	51.23±0.81

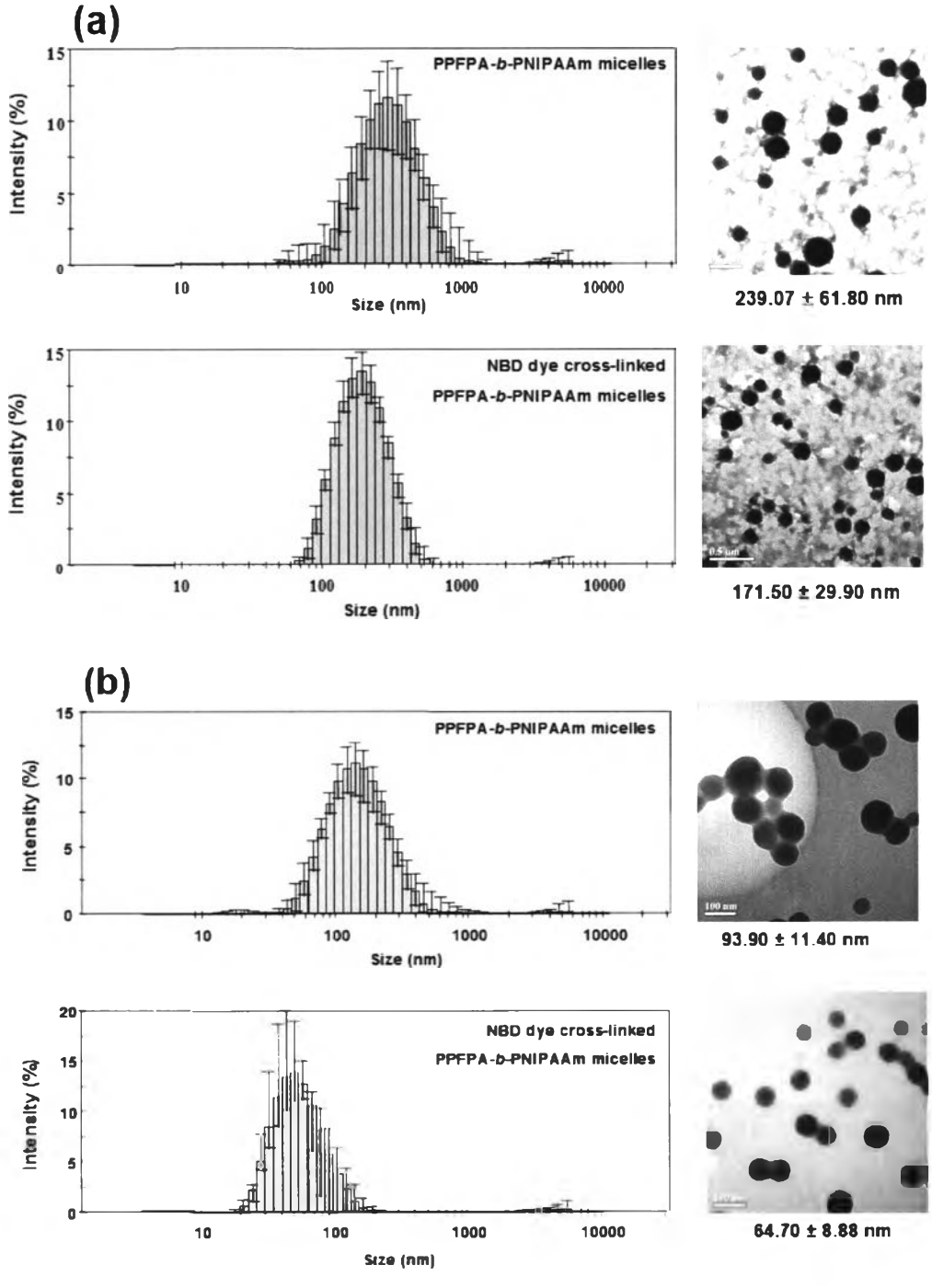

Figure 4.15. Size distribution profiles evaluated by DLS (left column) and TEM images (right column) of the PPFPA-*b*-PNIPAAm micelles and the NBD dye cross-linked micelles formulated from the copolymer with PPFPA:PNIPAAm composition of (a) 23:77, and (b) 71:29. DLS measurements were carried out at 10°C and a micelle concentration of 1 mg/mL.

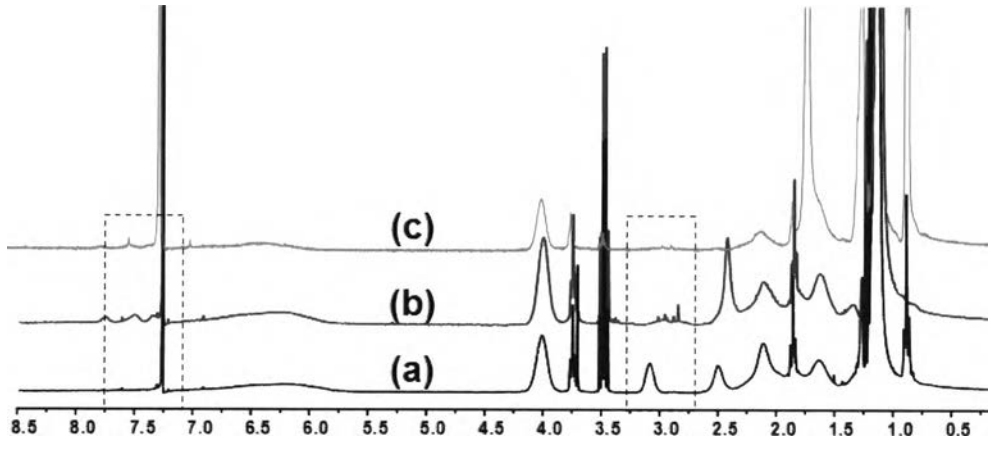

Figure 4.16. ^{1}H NMR spectra of (a) PPFPA-*b*-PNIPAAm, (b) ONB containing the PPFPA-*b*-PNIPAAm, and (c) NBD dye cross-linked PPFPA-*b*-PNIPAAm in $CDCl_3$.

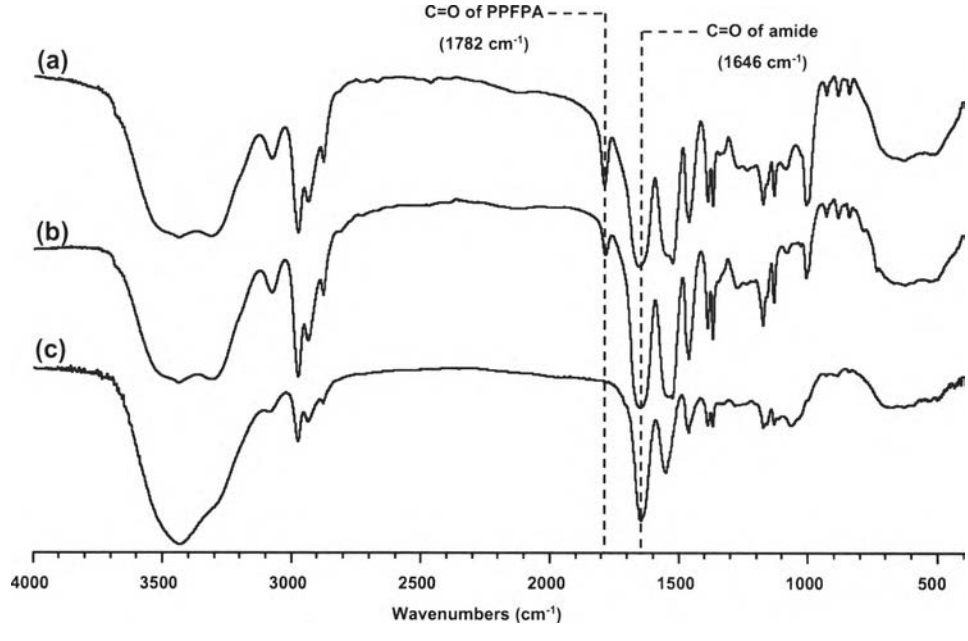

Figure 4.17. FTIR spectra of (a) PPFPA-*b*-PNIPAAm, (b) ONB containing the PPFPA-*b*-PNIPAAm, and (c) NBD dye cross-linked the PPFPA-*b*-PNIPAAm.

UV-Vis spectroscopy was used to confirm the addition of NBD dye into the core of micelles via post functionalization modification of the residual PPFPA units. As seen in Figure 4.18, an absorbance of free NBD appears at λ_{max}= 478 nm, which is corresponding to an absorbance of NBD cross-linked micelles. Furthermore, the

loading of pyrene dye into the core of the cross-linked micelles was also determined as shown in Figure 4.19. The typical UV-Vis spectrum of pyrene-loaded micelles is similar to that of free pyrene, suggesting no significant change in the structure of pyrene encapsulated in the core cross-linked micelles.

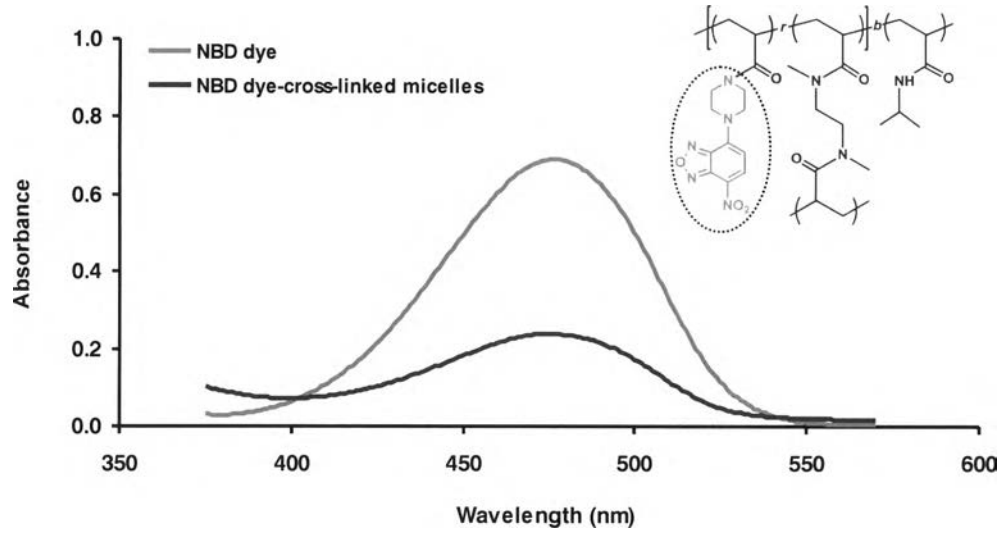

Figure 4.18. Absorbance of NBD dye and the NBD dye-cross-linked micelles.

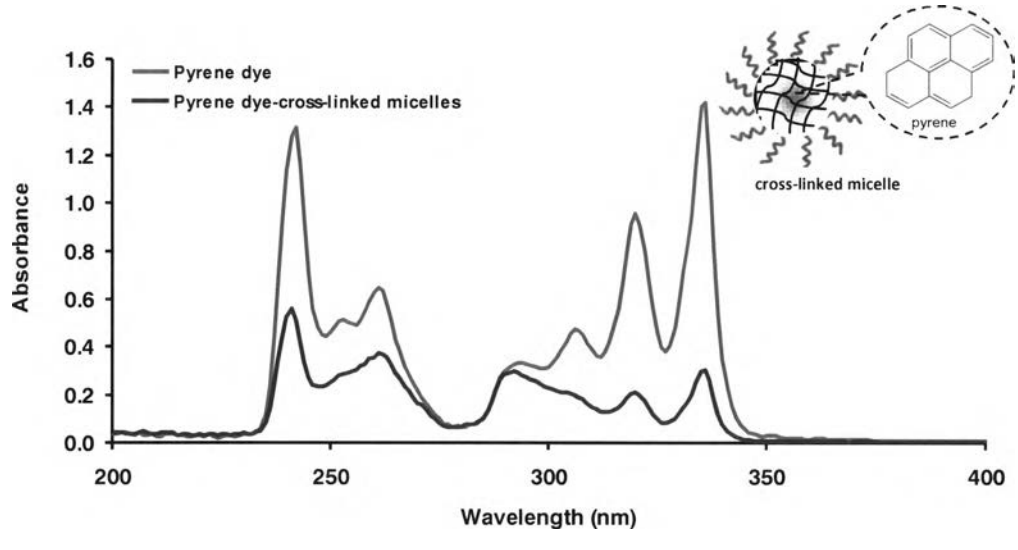

Figure 4.19. Absorbance of pyrene dye and the cross-linked micelles loaded with pyrene dye.

4.6 Formation of fiber by electrospinning technique

In this part, random copolymers of P(NIPAAm-*r*-PPFPA) and P(NIPAAm-*r*-NAS) were fabricated as fibers by electrospinning technique. The effect of polymer solution concentration, molecular weight, solvent, needle diameter was evaluated in order to get uniformed fibers for further cell study in the next part.

4.6.1 Electrospinning of P(PPFPA-*r*-NIPAAm) copolymer

4.6.1.1 Effect of solvent

In this study, P(NIPAAm-*r*-PPFPA) copolymer having M_n of 47 kDa was electrospun from THF and a binary solvent mixtures of THF/DMF (3:1 v/v) to study the effect of solvent towards the formation of fibers (Figure 4.20). For each solvent system, the polymer solution concentration was varied from 10 to 30% (w/v). The fibers electrospun from THF showed only beads and bead with some fibers on the collector at polymer solution concentration of 10 and 20% w/v, respectively. The average diameter of the fibers electrospun from THF at 30% w/v was 2.02 ± 0.84 μm. The fibers electrospun from the binary solvent mixtures of THF/DMF (3:1 v/v) formed beads with fibers at a polymer solution concentration of 30% w/v. Moreover, the average diameter fibers spun from the THF/DMF had smaller diameter than that of the fibers spun from THF. DMF is a polyelectrolytic solvent with relatively high dielectric constant (36.4) as compared to that of THF (7.6). The primary effect of using DMF instead of other electrically poor solvents is the reduction in fiber diameter due to increased elongational force within the solution jet [30]. Therefore, the binary solvent mixtures of THF/DMF (3:1 v/v) were used for further electrospinning of the P(NIPAAm-*r*-PPFPA).

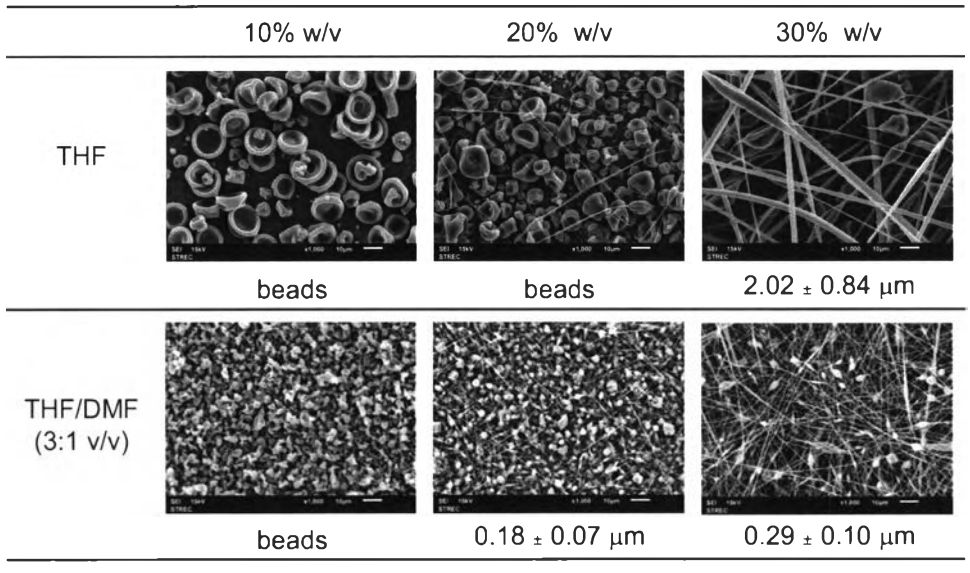

Figure 4.20. SEM micrographs of P(NIPAAm-*r*-PPFPA) fibers electrospun from THF and a binary mixture of THF/DMF (3:1) with different polymer concentrations from 10 to 30% w/v at a constant voltage of 20 kV, a flow rate of 3 mL/h. Number appearing below each micrograph is an average diameter of the electrospun fibers.

4.6.1.2 Effect of molecular weight and polymer solution concentration

The molecular weight and polymer solution concentration are the important parameters that pose strong impact on fiber formation. Figure 4.21 shows SEM micrographs of P(NIPAAm-*r*-PPFPA) electrospun fibers fabricated from two molecular weights (47 kDa and 60 kDa) with different polymer concentrations (10 to 30% w/v) at a constant voltage of 20 kV and a flow rate of 3 mL/h. As can be seen, the formation of fibers increased with elevated polymer concentrations and molecular weight of the polymers. At 10% w/v of polymer concentration and M_n of 47 kDa, only beads were formed on the collector due to little chain entanglement and low viscosity, while beads with some fibers appeared for the polymer with M_n of 60 kDa. At 20% w/v and M_n of 47 kDa, beaded fibers were formed and the fiber diameter was 0.18 ± 0.07 μm. In contrast, the fibers with fewer beads were formed for the polymer with M_n of 60 kDa. As the concentration of polymer in solution was increased, chain entanglement also increased and therefore enabled the polymer to

be electrospun. Therefore, the optimal molecular weight and polymer concentration of the P(PPFPA-*r*-NIPAAm) are 60 kDa and 30 w/v%, respectively. Moreover, the fiber diameters of the P(NIPAAm-*r*-PPFPA) were increased with increasing polymer concentration from 10 to 30% w/v range from 0.33 ± 0.13 to 0.62 ± 0.16 μm.

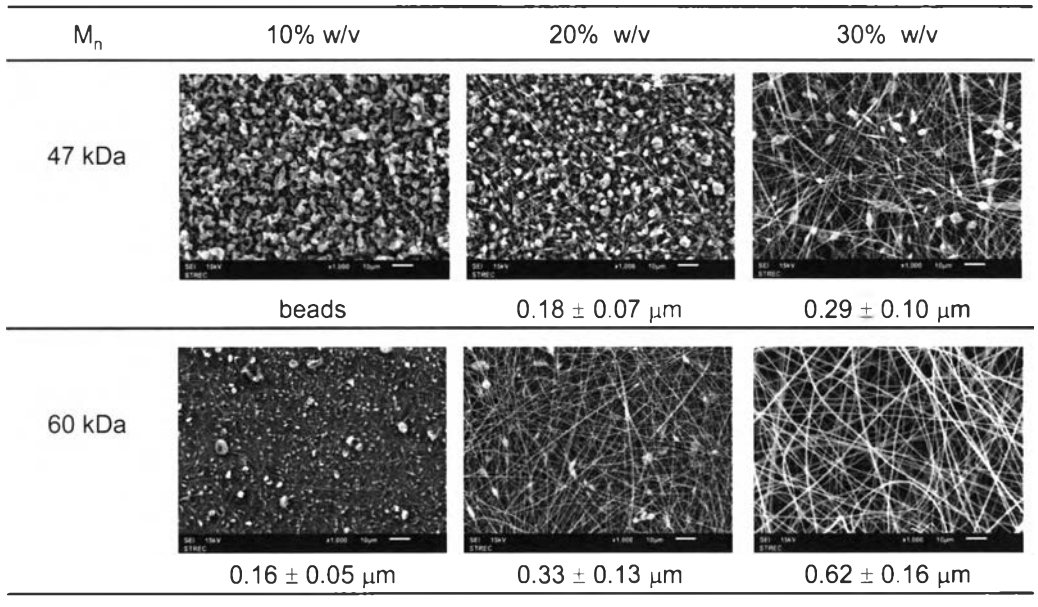

Figure 4.21. SEM micrographs of P(NIPAAm-*r*-PPFPA) fibers electrospun from two molecular weights (47 kDa and 60 kDa) with different polymer concentrations from 10 to 30% w/v at a constant voltage of 20 kV, a flow rate of 3 mL/h. Number appearing below each micrograph is an average diameter of the electrospun fibers.

4.6.1.3 Stability of uncross-linked and cross-linked P(PPFPA-*r*-NIPAAm) fibers

The stability of the cross-linked and uncross-linked P(NIPAAm-*r*-PPFPA) electrospun fiber mats were studied in BSA-FITC solution or phosphate-buffered saline (10 mM PBS, pH 7.4). Samples were immersed in the solutions for 24 h at room temperature and then washed with distilled water twice, followed by drying overnight under ambient conditions and then vacuum dried for another 24 h. The morphological changes in the samples were observed by SEM. The fiber diameters were measured on at least 50 samples to evaluate swelling of the fibers. The morphological changes and the diameters of the electrospun fibers before and after

treatment with the solutions are shown in Figure 4.22. Before immersion, all the samples were of similar diameters (around 600-700 nm). After immersion in the solutions for 24 h, both of the uncross-linked and cross-linked electrospun fiber could maintain their fibrous structure, although the diameters of both fibers slightly increased as a result from swelling of PNIPAAm.

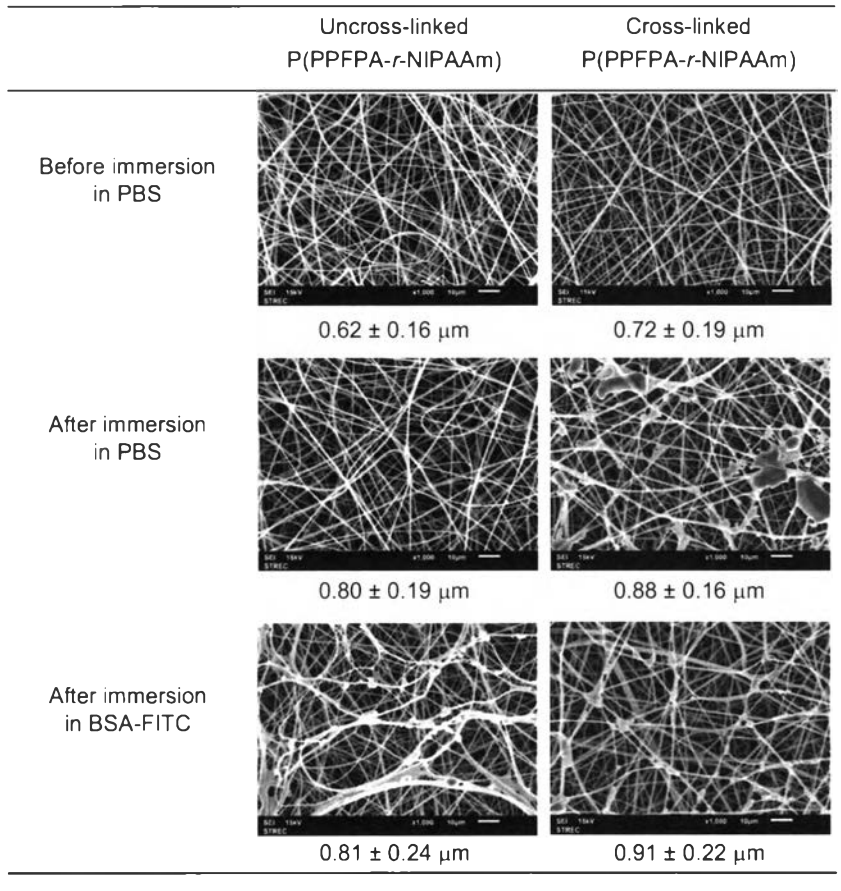

Figure 4.22. SEM micrographs of uncross-linked and cross-linked P(NIPAAm-*r*-PPFPA) fibers before and after immersion in PBS and BSA-FITC for 24 h.

4.6.2 Electrospinning of P(NIPAAm-*r*-NAS)

4.6.2.1 Effect of polymer concentration and needle diameter

The effects of polymer solution concentration and needle diameter on the resulting electrospun P(NIPAAm-*r*-NAS) having $M_{n,th}$ of 133 kDa were evaluated and reported in this section. Figure 4.23 shows SEM images of the electrospun P(NIPAAm-*r*-NAS) fibers obtained with different processing conditions. At the polymer

concentrations of 10 % (w/v), defects in the form of beads were observed. Increasing the solution viscosity so as the chain entanglement by increasing the polymer concentration to 20% (w/v) yielded fibers with fewer beads. At a concentration of 30% (w/v), fibers exhibited flat surface morphologies. The average fiber diameters at a concentration of 30% (w/v) were calculated as 4.03 ± 1.20 μm and 2.20 ± 0.72 μm for the needle diameter of 0.7 and 0.5 mm, respectively, which clearly confirmed that fiber diameter significantly decrease with the decrease of needle diameter.

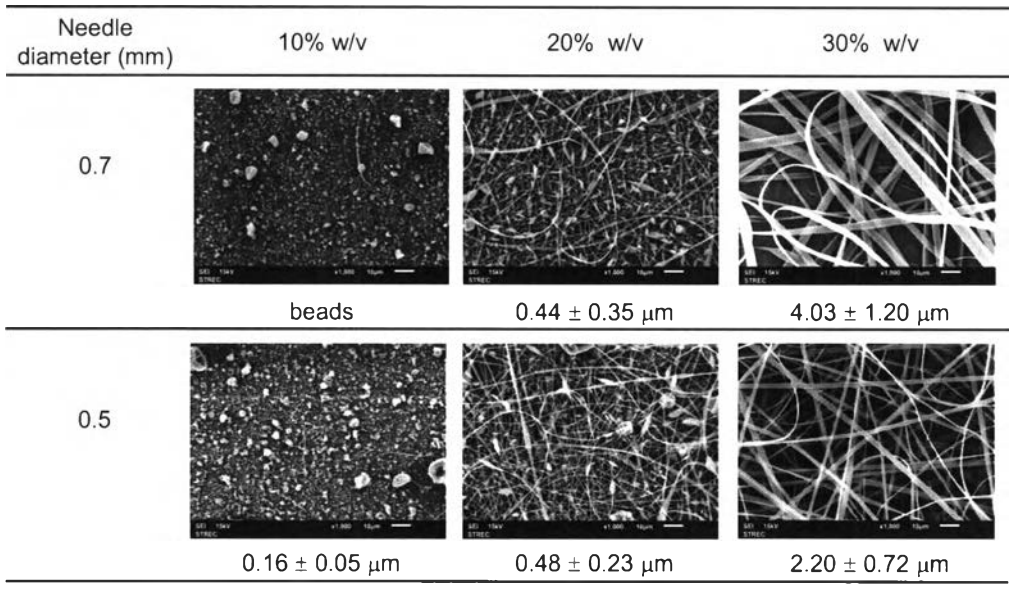

Figure 4.23. SEM micrographs of P(NIPAAm-*r*-NAS) fibers electrospun from needle having two different diameters (0.5 and 0.7 mm) of polymer solution having varied concentration from 10 to 20 and 30% (w/v) at a constant voltage of 20 kV and a flow rate of 3 mL/h.

4.6.2.2 Cross-linked P(NIPAAm-*r*-NAS) fibers

Herein, light responsive moieties of ONB containing random P(NIPAAm-*r*-NAS) having the ONB group substitution of 21.9% were electrospun as fibers. Figure 4.24 shows SEM images of the ONB containing P(NIPAAm-*r*-NAS) fibers before and after UV irradiation at 365 nm. At 30% (w/v), fibers were formed and the average fiber diameter of uncross-linked fibers was 0.75 ± 0.36 μm, while the cross-linked fibers had average diameters of 0.56 ± 0.27 μm. After UV irradiation, the diameter of the cross-linked fibers were found to be smaller than those of the uncross-linked

fibers implying that covalently cross-linked network of ONB-protected amine with the NAS part were formed.

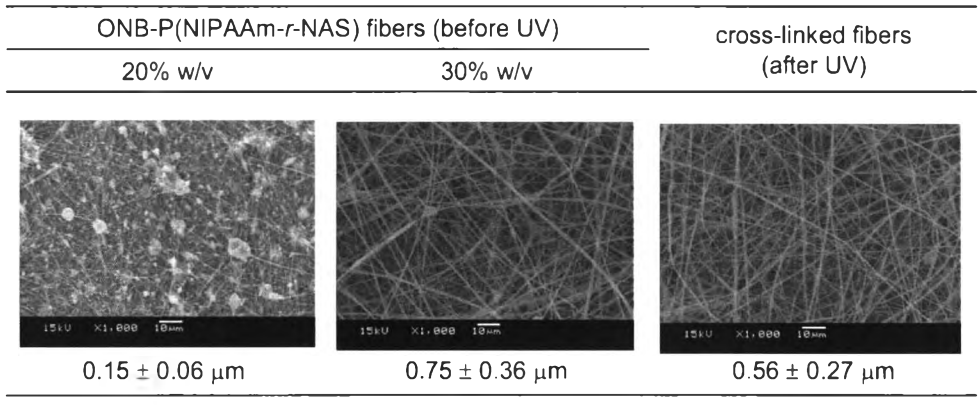

Figure 4.24. SEM micrographs of P(NIPAAm-*r*-NAS) fibers electrospun from the polymer solution of 30% (w/v) at a constant voltage of 20 kV and a flow rate of 3 mL/h.

4.6.2.3 Stability of uncross-linked and cross-linked P(NIPAAm-*r*-NAS) fibers

The physical stability of the uncross-linked and cross-linked electrospun P(NIPAAm-*r*-NAS) fibers were studied in both of BSA-FITC solution and phosphate-buffered saline (10 mM PBS, pH 7.4). Samples were immersed in the solutions for 24 h at room temperature. The morphological changes and the diameters of the electrospun fibers before and after the treatment are shown in Figure 4.25. As can be seen, the cross-linked P(NIPAAm-*r*-NAS) fibers became interconnected fibers, whereas the uncross-linked P(NIPAAm-*r*-NAS) fibers could not maintain their fibrous structure, suggesting that both of uncross-linked and cross-linked P(NIPAAm-*r*-NAS) fibers are not suitable for practical usage due to the hydrolytic unstability of the NAS groups.

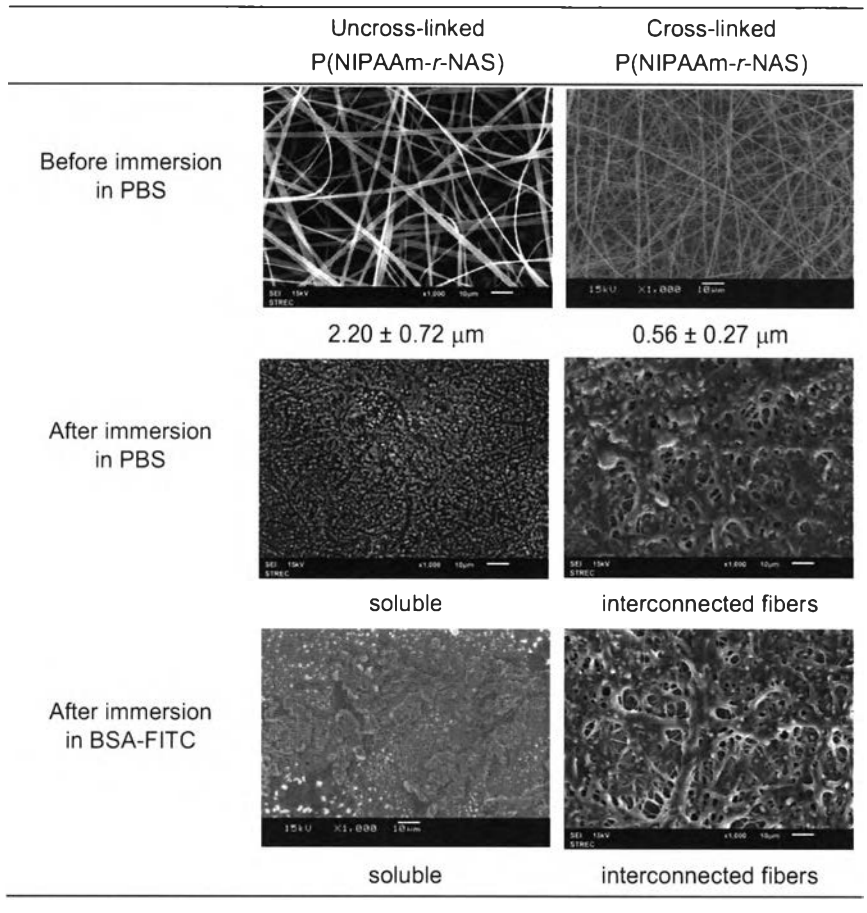

Figure 4.25. SEM micrographs of uncross-linked and cross-linked P(NIPAAm-*r*-NAS) fibers before and after immersion in PBS and BSA-FITC for 24 h.

4.7 Immobilization of GRGDS peptide on the P(NIPAAm-*r*-PPFPA) fibers

Prior to immobilization of GRGDS peptide on both uncross-linked and cross-linked fibrous surfaces, Albumin-fluorescein isothiocyanate conjugate (BSA-FITC) was used as a fluorescent-labeled biomolecule model to prove whether or not amino-containing molecules can react with the active ester groups of PFPA units in the copolymer. Figure 4.26 shows fluorescence images of uncross-linked and cross-linked P(NIPAAm-*r*-PPFPA) fibers implying the successful immobilization of the BSA-FITC onto the fibers. Dye distribution was homogeneous along the fibers. This result also implies a homogeneous distribution of PPFPA moieties of the P(NIPAAm-*r*-PPFPA) random copolymer on the fiber surfaces. Furthermore, the obvious change of water

contact angle during functionalization of the GRGDS peptide on the fibrous surfaces was confirmed by water contact angle measurement. As expected, the water contact angles of both uncross-linked and cross-linked fibers (shown in Table 4.5) significantly decreased after reacting with GRGDS peptide, indicating that some of hydrophobic moieties of PFPA units have been replaced by the more hydrophilic GRGDS peptide.

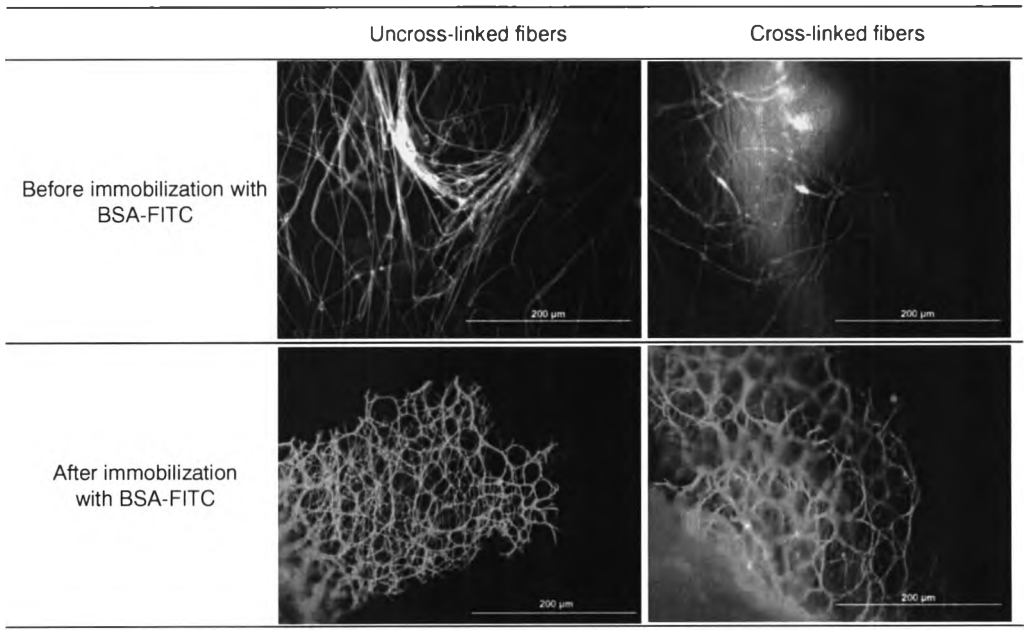

Figure 4.26. Fluorescence micrographs of uncross-linked and cross-linked P(NIPAAm-*r*-PPFPA) fibers before and after immobilization with BSA-FITC.

Table 4.5 Water contact angles of uncross-linked and cross-linked P(NIPAAm-*r*-PPFPA) before and after immobilization of GRGDS peptide.

Sample name	Water contact angle before immobilization of GRGDS (degree)	Water contact angle after immobilization of GRGDS (degree)
Uncross-linked fibers	157.6 ± 8.33	105.6 ± 4.16
Cross-linked fibers	129.2 ± 6.29	80.3 ± 2.93

4.8 Cytocompatibility test

The Arg-Gly-Asp (RGD)-containing peptide is well known for its ability to promote cellular attachment by binding to integrin receptors on cell surface. The

peptide sequence RGD found in fibronectin, type I collagen, and other extracellular matrix (ECM) proteins has been widely studied as an immobilized cell adhesion ligand specific for integrin-mediated cell adhesion. This interaction was also shown to play an important role in cell growth, differentiation, and overall regulation of cell functions [31].

Cell adhesion, spreading and migration on substrates are the first sequential reactions when coming into contact with a material surface, which is crucial for cell survival. The cellular behavior on biomaterials is an important factor for evaluation of the biocompatibility of biomaterial. Fibroblast is a type of cell, which synthesizes the ECM and collagen, which is the structural framework for animal tissues.

In this research, the *in vitro* cytocompatibility of GRGDS-immobilized uncross-linked (abbreviated as GRGDS-UC) and GRGDS-immobilized cross-linked (abbreviated as GRGDS-C) of P(NIPAAm-*r*-PPFPA) fibers was carried out against mice L929 fibroblast cell line. To investigate the mitochondrial functions of the cultured L929, reduction of MTT reagent was used as an assay of mitochondrial redox activity. MTT reagent is a pale yellow substance that is reduced to a dark blue formazan product when incubating with viable cells by mitochondrial succinate dehydrogenase in complex II, which plays a critical role in both oxidative phosphorylation and tricarboxylic acid cycle. Therefore, the production of formazan can reflect the level of cell viability.

For cell culture assay, the fibers were treated with UV light before cell seeding for 12 h. $2x10^4$ cells were directly seeding on each fibers surface in 24-well tissue culture plate. The tissue culture plate after cell seeding was incubated in a humidified environment at $37^{\circ}C$ and with 5% CO_2 supply. The cell adhesion was determined at 6 h and cell proliferation was evaluated at 1 day, 3 days and 5 days of cell culture. The results are reported in terms of the cell adhesion and proliferation ratio (% relative to TCPS) which is directly correlated to the number of viable cells.

After 6 h of cell culture, the cell adhesion ratio (% relative to TCPS) on GRGDS-UC, and GRGDS-C fibers were 60 and 109%, respectively. The percent cell adhesion ratio became higher after the fibers were immobilized with the GRGDS indicating that the GRGDS peptide support cell adhesion at 6 h (Figure 4.27). We explain the inferior cellular adhesion in both un-cross-linked and cross-linked fibers

before peptide immobilization as a consequence of the hydrophobic nature of the fibers as opposed to the TCPS and the fibers after peptide immobilization. Apparently, the degree of cell adhesion corresponded well with the hydrophobicity of the fibers (See water contact angle data in Table 4.5)

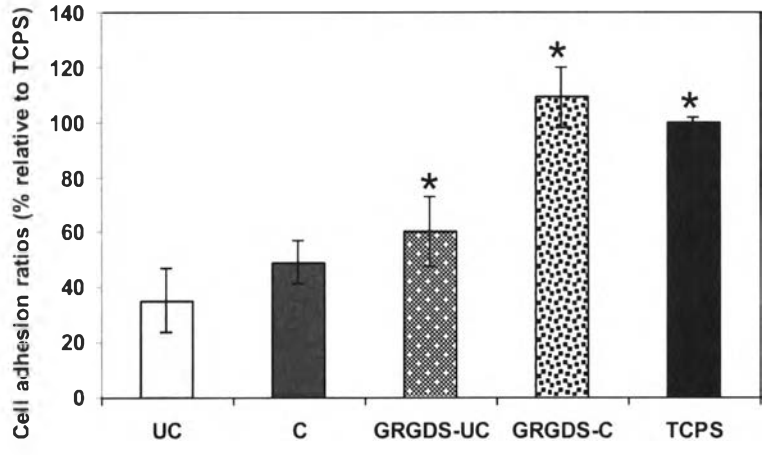

Figure 4.27. Cell adhesion ratios (% relative to TCPS) of L929 cells at 6 h with a seeding density of 2.0 x 10^3 cells/well on uncross-linked (UC), cross-linked (C), GRGDS-immobilized uncross-linked (GRGDS-UC) and cross-linked fibers (GRGDS-C), and TCPS. *$P < 0.05$ (compared to control: UC and C).

Cell proliferation was checked on 1 day, 3 days, and 5 days of cell culture. The data of cell proliferation ratio (% relative to TCPS) are displayed in Figure 4.28. The percent of live cells increases with an increase in cell culture time. The percent of live cells for GRGDS-C fibers was higher than those of GRGDS-UC fibers. This outcome suggested that not only peptide but also hydrophilicity of surfaces an important parameter that dictates cell growth.

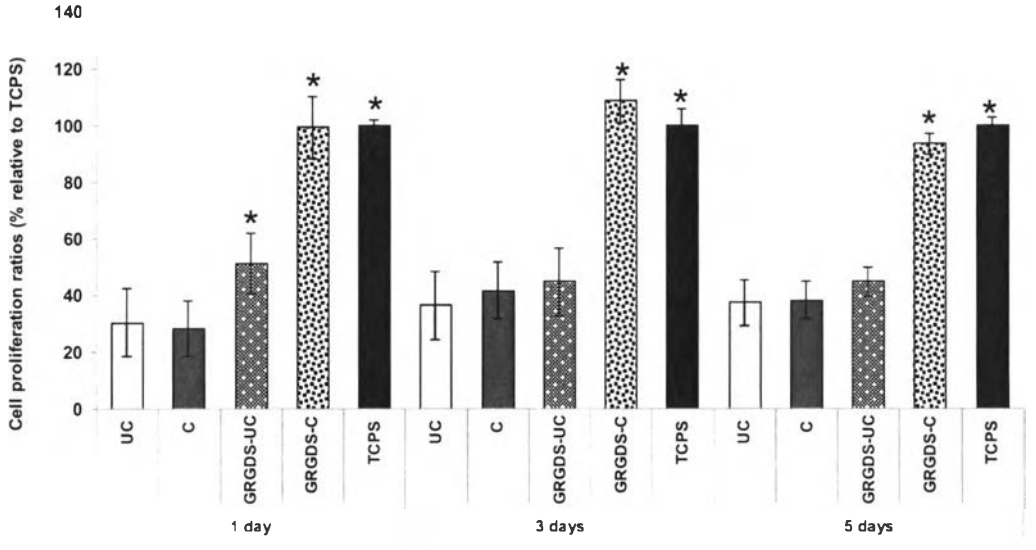

Figure 4.28. Cell proliferation ratios (% relative to TCPS) of L929 cells at 1, 3, and 5 days with a seeding density of 2.0×10^3 cells/well on uncross-linked (UC), cross-linked (C), GRGDS-UC and GRGDS-C fibers, and TCPS. *$P < 0.05$ (compared to control: UC and C).

For cell detachment treatment, spread cells were transferred to an incubator equipped with a cooling unit fixed at 20°C. The morphology of both attached and detached cells were observed by SEM. When the culture temperature was reduced to 20°C after incubation at 37°C for a set of time, the spread cells became rounded and detached from both GRGDS-UC and GRGDS-C surfaces. Spread cells were more slightly detached from GRGDS-C surfaces than GRGDS-UC surfaces. This is because the GRGDS-C surfaces are more hydrophilic than that of the GRGDS-UC surfaces. In addition, Ebara *et al.*[32], reported that at temperatures below the grafted polymer's LCST, integrin-RGDS association decreases due to loss of cell tension and surface anchoring, prompting cells to round and then detach. This surface property changes weakened cellular adhesion, resulting in spontaneous cell detachment as shown in Figure 4.29-4.30.

Biocompatibility is the main requirement for any polymeric synthetic materials to be useful in tissue engineering. It should not leach any toxic substances that may cause harm to cells or otherwise interfere with the physiological responses

of the cells that come in contact with these substances. Moreover, initial cell attachment, rapid proliferation, and rapid intact cell recovery are important to maintain biological functions and viability of cell source for the fields of regenerative medicine. From this view point, the GRGDS-C fibers could be a promising biomaterial to recover intact cultured cells for cell culture and tissue engineering applications.

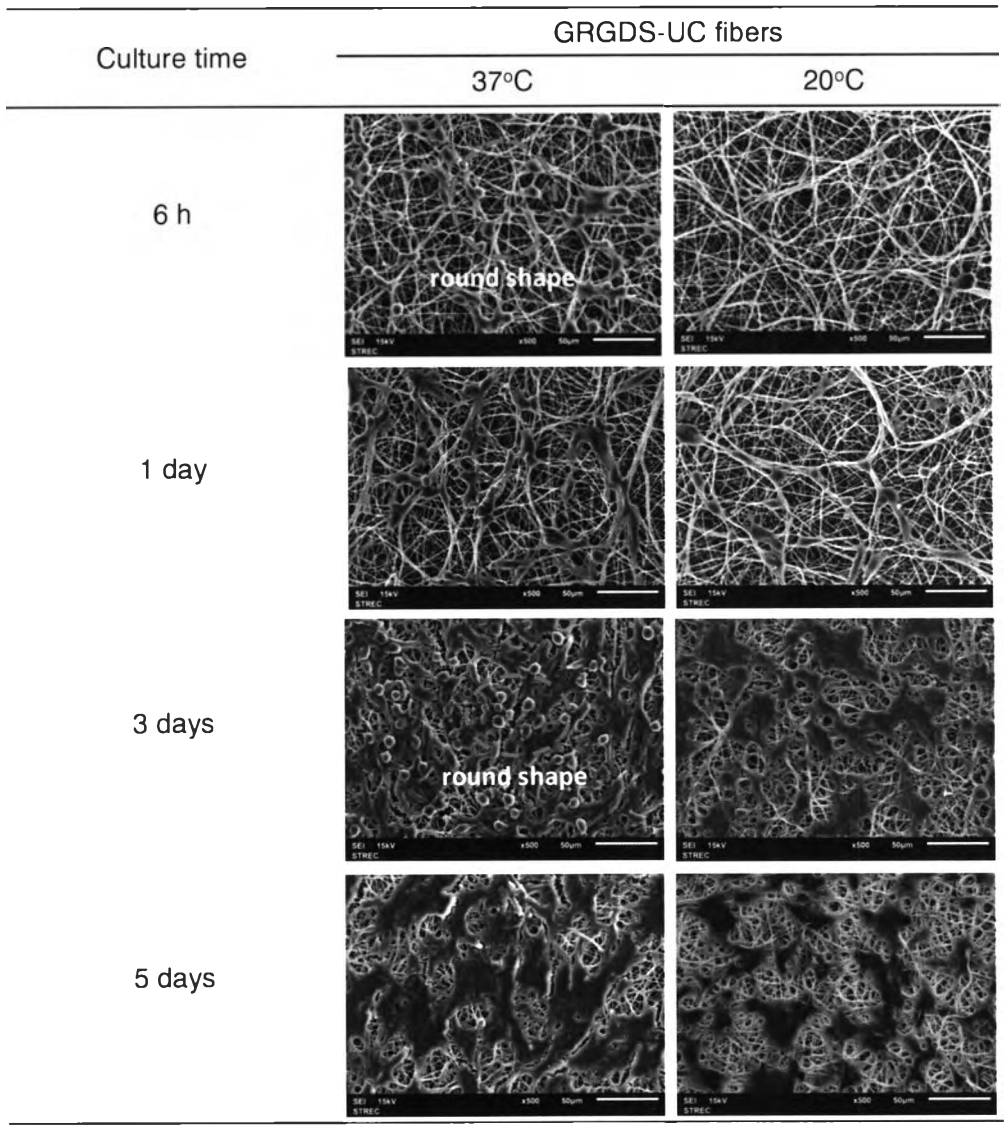

Figure 4.29. SEM micrographs of fibroblasts on the GRGDS-UC fibers: attachment at 37°C (left column) and detachment at 20°C (right column) for a set culture time.

Culture time	GRGDS-C fibers	
	37°C	20°C
6 h	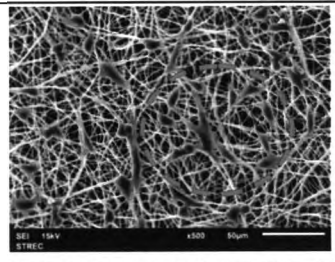	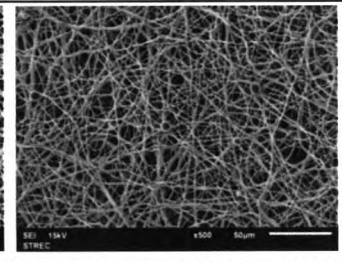
1 day	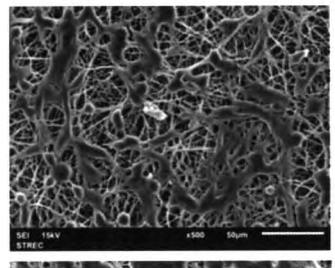	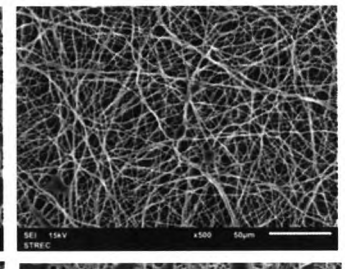
3 days	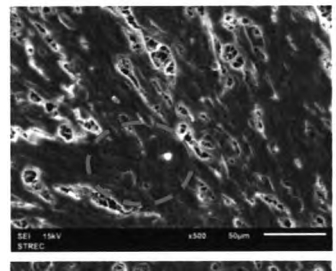	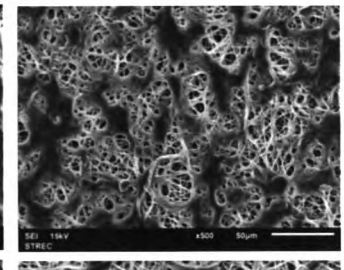
5 days	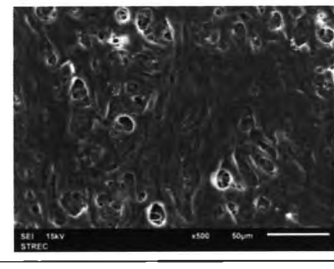	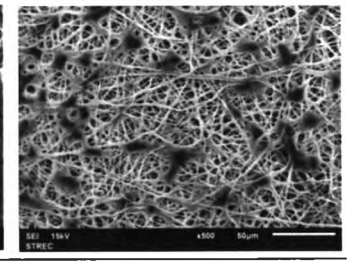

Figure 4.30. SEM micrographs of fibroblasts on the GRGDS-C fibers: attachment at 37°C (left column) and detachment at 20°C (right column) for a set culture time.